IEEE Access
Multidisciplinary ⋮ Rapid Review ⋮ Open Access Journal

Received April 30, 2020, accepted May 19, 2020, date of publication May 25, 2020, date of current version June 9, 2020.

Digital Object Identifier 10.1109/ACCESS.2020.2997125

Development of a New Multifunctional Induced Polarization Instrument Based on Remote Wireless Communication Technology

WENHAO LI[1], QISHENG ZHANG[1], YUEYUN LUO[1], QIMAO ZHANG[2], AND FEI JIANG[3]

[1]School of Geophysics and Information Technology, China University of Geosciences (Beijing), Beijing 100083, China
[2]Institute of Electronics, Chinese Academy of Sciences, Beijing 100049, China
[3]School of Earth and Space Sciences, University of Science and Technology of China, Hefei 230026, China

Corresponding author: Qisheng Zhang (zqs@cugb.edu.cn)

This work was supported in part by the Natural Science Foundation of China under Grant 41574131, in part by the National Key Research and Development Program of China under Grant 2017YFF0105704, in part by the National 863 Program of China under Grant 2012AA06110203, in part by the PetroChina Innovation Foundation under Grant 2019D-5007-0302, and in part by the Fundamental Research Funds for the Central Universities of China.

ABSTRACT Induced polarization (IP) is the primary method used for the exploration of various metal minerals and for groundwater prospecting. The function and performance of IP instruments have significantly improved over the years; however, most instruments still have some shortcomings, such as limited data acquisition accuracy, large size, separate transmitter and receiver, complex human–computer interaction, difficult networking and remote monitoring. In this study, a novel multifunctional IP instrument system is developed based on remote wireless communication technology, which has high data acquisition accuracy, small size, lightweight, flexible and diverse functions (single instrument can realize transmission and reception), remote wireless real-time monitoring, and convenient networking of multiple instruments. We independently designed a high-precision data acquisition circuit with a noise floor of 0.29 μV and a 5-fold increase in acquisition accuracy. With an intelligent power module as its core, the designed transmitter has a maximum output power of 6 kW and can transmit stepped waves and rectangular waves of various frequencies and duty cycles. We also developed a host computer program on an Android mobile terminal based on Java, which allows users to wirelessly control the instrument through mobile phones over Wi-Fi networks. In addition, we introduced the Internet of Things technology in geophysical instruments and designed a real-time remote monitoring system for data quality and multiple instruments networking scheme based on the short message service of the BeiDou navigation satellite system and cloud service platform. Multiple tests revealed that the proposed instrument meets the requirements of field exploration.

INDEX TERMS Cloud service platform, data acquisition, induced polarization instrument, Wi-Fi communication.

I. INTRODUCTION

Electrical prospecting is widely used in geological exploration and engineering inspection owing to its diverse applicability and tools [1], [2]. Induced polarization (IP) is an electrical prospecting method based on the differences in the IP effects of different rocks and minerals for ore prospecting and geological exploration to study the distribution of artificial DC (time domain) or AC (frequency domain) IP fields [3]–[5]. Compared with the resistivity method and the electromagnetic method, the IP method is more advantageous for exploring disseminated metal ore deposits with small differences in resistivity from the surrounding rocks. Field practices have demonstrated that the IP method can also achieve satisfactory results in the exploration of energy sources, such as petroleum and natural gas, and detection of groundwater. Currently, the IP method is the primary method used for exploring various metal minerals and detecting groundwater [6]–[9].

Advanced geophysical instruments, such as IP instruments and seismographs, are very important for investigating geoscience problems [10]. With the development and

The associate editor coordinating the review of this manuscript and approving it for publication was Adnan M. Abu-Mahfouz.

maturity of IP exploration and advancements in electronic, computer, and signal processing technology, IP instruments have also developed rapidly. Currently, representative IP measurement instruments worldwide include the GDP series multifunctional electrical prospecting instruments (Zonge International), V series electrical prospecting instruments (Phoenix Geophysics), KMS series exploration instruments (KMS Technologies), full-waveform (FW) high-power IP instruments (IRIS Instruments), IPR-12 (Scintrex), RESECS series (DMT Group), McOHM series (OYO Corporation), Horn3D full functional IP instruments (Crystal Globe), electrical prospecting instruments and IP instruments (Advanced Geosciences Inc.), and various electrical prospecting instruments developed by institutes such as Central South University, Jilin University, and the Chinese Academy of Sciences. Although the functions and performance of these IP instruments have generally improved significantly over the years, some shortcomings remain [11]–[16]. First, most of the above-mentioned instruments have only the functions of a receiver; they require an additional transmitter to complete field exploration work, which increases the difficulty and cost of exploration. In terms of human-computer interaction, some instruments (such as the SQ-5 dual-frequency IP instrument of Geosun Hi-Technology) [17] still use traditional buttons and LCD display screens, making their operation relatively complex and simultaneous configuration of multiple instruments difficult. Furthermore, the complexity of the exploration environment requires higher data acquisition accuracy and the use of lighter instruments. Some instruments have disadvantages such as limited acquisition accuracy and large weight (for example, the minimum input voltage of IPR-12 by Scintrex is 50 μV, with a resolution of 10 μV and weight of 7.1 kg) [18]. In terms of data transmission and quality monitoring, some instruments store data only on an internal SD card, which cannot realize real-time display of data and results. Other instruments (such as GDD DC IP instrument) use low-speed short-distance wireless communication technology, such as Bluetooth [19], which makes it difficult to realize real-time high-speed transmission of large amounts of data and remote wireless data quality monitoring.

In this study, we developed a novel multifunctional IP instrument based on remote wireless communication technology that integrates a high-power transmitter and a high-precision receiver, and can also be used independently. Field exploration can be performed using only the proposed instrument, which reduces the complexity of fieldwork. We achieved high-precision (in the order of several hundred nV) data acquisition using circuits and programs developed in our laboratory so that the instrument can adapt to the increasingly complex exploration environment. We introduced the Internet of Things (IoT) technology in geophysical instruments to realize distributed networking of multiple instruments to eliminate the complexity of operations of traditional human–computer interaction, and configure instrument parameters, control the operation of the instrument, monitor the data quality in real-time, and view the data processing results using Android devices. At the same time, users can also remotely monitor and control multiple instruments through the short message service (SMS) of the BeiDou navigation satellite system (BDS) or a cloud service platform. The proposed instrument has advantages of high integration, high data acquisition accuracy, multi-function capability, compact, lightweight, convenient operation, and a high degree of intelligence (details of the main indicators and comparison with similar instrument are presented in "F. PERFORMANCE SUMMARY AND COMPARISON" of Section IV).

The structure of this paper is as follows: Section II briefly introduces the basic theory of the IP method, Section III describes the overall composition of the system, the key technologies of the developed IP instrument system are described in Section IV, Section V presents the test results, and the main conclusions are summarized in Section VI.

II. BASIC THEORY OF THE IP METHOD

Fig. 1 shows a schematic diagram of an IP instrument. The transmitter injects current into the ground through electrodes A and B, and the receiver receives the potential difference signal generated by the ground medium at points M and N.

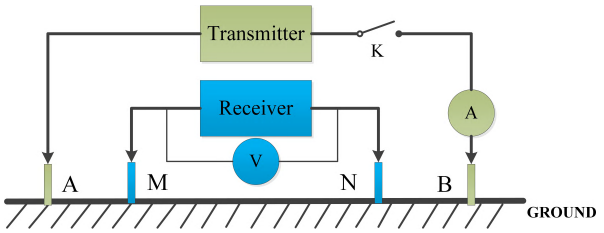

FIGURE 1. Schematic diagram of an induced polarization instrument (A (left) and B: transmitting electrodes; M and N: receiving electrodes; K: switch; V: voltmeter; A (right): ammeter).

If the medium is nonpolarized and the supply current remains constant, the potential difference V_1 between M and N is constant. If the ground medium is polarized, the medium undergoes an electrochemical reaction with the supply of current, resulting in a secondary potential difference V_2 between M and N. Polarization of the medium gradually decreases and saturates with time, and V_2 steadily stabilizes. When A and B stop supplying power to the ground, V_1 produced by the power supply disappears, whereas the secondary potential difference V_2 produced by the polarization of the medium does not disappear instantly; the dissipation rate is initially fast but slows with time, and V_2 gradually decreases until it disappears [20], [21]. The schematic curve of the charging and discharging processes described above is shown in Fig. 2.

III. OVERALL COMPOSITION OF THE IP INSTRUMENT SYSTEM

The overall composition of the IP instrument system is shown in Fig. 3, comprising the instrument host and mobile terminal

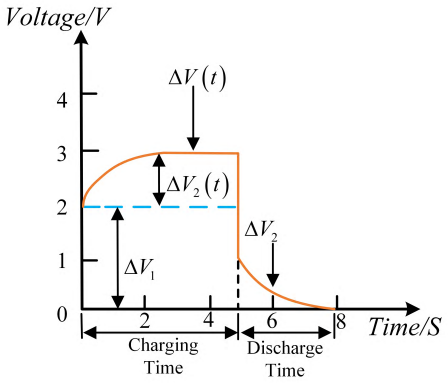

FIGURE 2. Charging and discharging curves of IP phenomenon in the time domain.

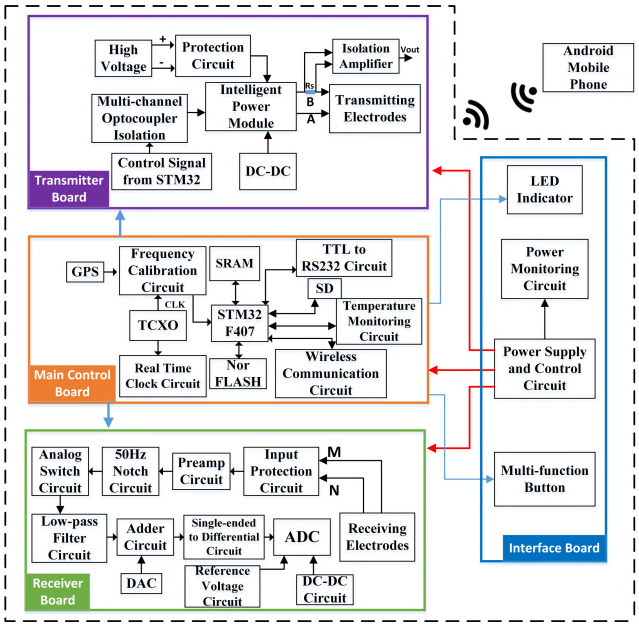

FIGURE 3. Overall composition of the IP instrument system.

control software. The instrument host has four modules: transmitter, master control, receiver, and interface boards. The first three circuit boards are connected to the interface board in parallel with high-performance connectors (Fig. 4). Users control the operation of the instrument and monitor the instrument status and data processing results through a Wi-Fi network.

The interface board is equipped with a system power supply unit and its control circuit, through which a user can control the power supply of the transmitter and receiver, in addition to monitoring the voltage, current, power, and battery levels of the system in real-time. LED lights are used to indicate the current operating status of the system. Users can also control the on/off states of the instrument and enter/exit the data acquisition state by pressing the appropriate keys.

The instrument uses STM32F407, SRAM, and Nor FLASH as the main control unit of the system. To improve the accuracy of data acquisition, we designed a frequency

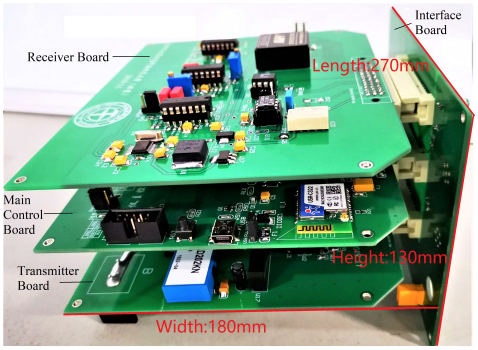

FIGURE 4. Photograph of the host circuit board of the IP instrument.

calibration circuit that uses a calibrated temperature compensated crystal oscillator (TCXO) as the clock. We used a global positioning system (GPS) and a BDS integrated positioning module to achieve high-precision synchronization of multiple instruments using the second pulse signal of the module. In addition, the unique SMS functionality of BDS provides a new option for remote data quality monitoring. Data collected by the instrument can be stored on an internal SD card; the original data and the processed results can be transmitted simultaneously to a mobile host terminal through a wireless communication circuit for real-time viewing by users. Users can debug and troubleshoot the instrument through the reserved RS232 interface and monitor its internal temperature in real-time using a temperature monitoring circuit to prevent unnecessary losses caused by high temperatures.

IV. KEY TECHNOLOGIES

A. HIGH-PRECISION DATA ACQUISITION BOARD

The functional block diagram of the data acquisition board shown in Fig. 3 primarily comprises signal conditioning, analog-to-digital conversion, and power conversion circuits. To reduce interference and noise, and improve the accuracy of data acquisition, we employed a separate power supply and single-point grounding for the analog and digital circuits and separately equipped the analog-to-digital converter (ADC) with a low-temperature drift and a low-noise precision voltage reference chip. We designed the signal front-end conditioning circuit, whose schematic is shown in Fig. 5, based on the characteristics of the output signal of the receiving electrodes M and N. To increase the input impedance, the signal first enters the instrument amplifier LT1168 after passing through the front-end protection circuit, and then passes through the analog switch ADG419 and a 50 Hz notch filter was used when necessary. The Sallen–Key (SK) unity-gain low-pass filter designed in this study was used to filter the high-frequency noise in the signal [22], and the adder circuit was primarily used for spontaneous potential compensation. Users can choose to compensate according to the actual exploration requirements. Finally, the signal is converted to a differential signal, which is fed into the ADC for analog-to-digital conversion, to improve the common-mode rejection ratio (CMRR).

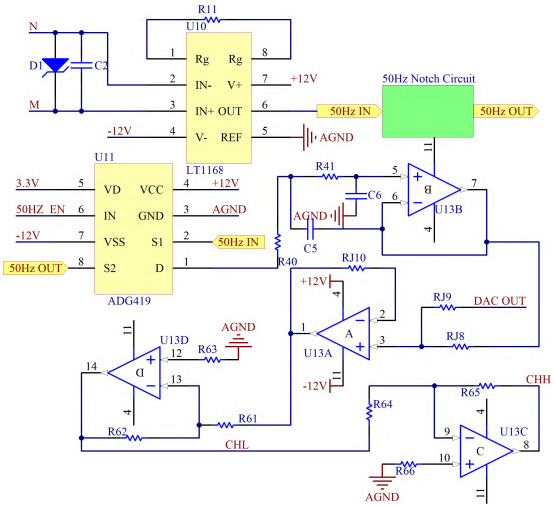

FIGURE 5. Circuit diagram of the signal conditioning circuit.

The noise floor of the acquisition circuit is closely related to the data acquisition accuracy of the instrument. The signal input terminal was short-circuited to verify the performance of the acquisition circuit, and the sampling rate was configured to 1000 samples per second; data were collected for a period of time, followed by calculation, and analysis using MATLAB. The proportion of the noise floor amplitude distribution within 10 s is shown in Fig. 6. The figure shows that most of the noise is below 1 μV, and the average noise is 0.29 μV, indicating that the accuracy of the acquisition circuit is extremely high compared with that of the previous version of the circuit, which satisfies the actual operating requirements of the instrument.

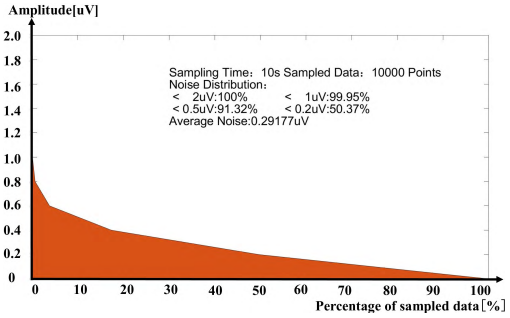

FIGURE 6. Proportion of noise floor distribution.

B. 50 Hz FILTER CIRCUIT

In practice, the 50 Hz utility frequency significantly affects the instrument operation and exploration results. Therefore, effective measures must be implemented in the instrument design to reduce the effect of this interference on the acquired signal [23]. In this study, we combined an analog hardware filter circuit with a digital software filter to reduce the interference of the utility frequency. In the hardware circuit, a 50 Hz filter circuit with excellent performance was

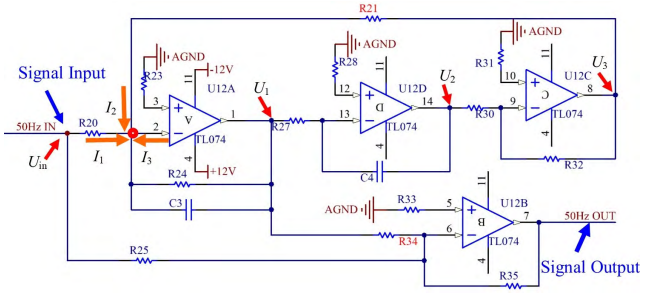

FIGURE 7. Circuit diagram of the 50 Hz filter circuit.

constructed with low-cost operational amplifiers TL074 and resistor-capacitors (Fig. 7).

The detailed analysis of the frequency selection circuit, based on the KCL principle [24], is as follows:

$$I_1 + I_2 + I_3 = 0, \tag{1}$$

where

$$I_1 = \frac{U_{in}}{R_{20}}; \tag{2}$$

$$I_2 = \frac{U_3}{R_{21}}; \tag{3}$$

$$I_3 = \frac{U_1}{R_{24}//(\frac{1}{j\omega C_3})}; \tag{4}$$

$$\frac{U_2}{U_1} = -\frac{1}{j\omega C_4 R_{27}}; \tag{5}$$

$$\frac{U_3}{U_2} = -\frac{R_{32}}{R_{30}}. \tag{6}$$

According to (1)–(6),

$$\frac{U_1}{U_{in}} = -\frac{1}{\frac{R_{20}}{j\omega R_{21} R_{27} C_4} + 1 + j\omega R_{20} C_3} \quad (C_3 = C_4, R_{30} = R_{32}, R_{20} = R_{24}). \tag{7}$$

When (7) reaches its maximum value, the degree of attenuation of the filter circuit to the 50 Hz signal also reaches its maximum. Next, we performed a frequency sweep analysis on the filter circuit in the 1–100 Hz range; the amplitude–frequency characteristic curve was evaluated and plotted using MATLAB (Fig. 8). The attenuation of this circuit to the 50 Hz signal was higher than 40 dB. After applying the digital filter in the program, the attenuation of the 50 Hz signal reached 80 dB, which satisfies the actual operating requirements.

C. MULTIFUNCTION TRANSMITTER BOARD

The DC IP method and the AC IP method have their respective advantages and disadvantages: the DC IP method is superior in terms of exploration depth and mitigation of electromagnetic coupling interference, whereas the AC IP method has a strong anti-interference capability and more parameters can be observed and studied. Therefore, the type of IP method should be selected for a specific working area

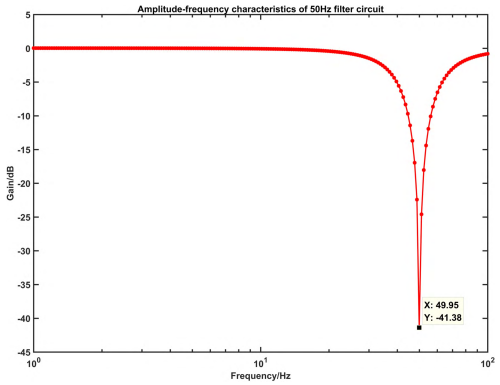

FIGURE 8. Amplitude–frequency characteristic curve of the 50 Hz filter circuit in practice.

considering the geological tasks, topography of the working area, and various interference conditions [25], [26]. In this study, we designed a multifunctional transmitter board with an intelligent power module (IPM) to transmit step waves (time domain) or rectangular waves (frequency domain) with various frequencies and duty cycles. The transmitter board primarily comprises a high-voltage power supply, a control circuit, IPM, a power conversion circuit, and a transmitting electrode (Fig. 3). The high-voltage power supply passes through a protection circuit and provides an adjustable voltage for the input terminal of the IPM to meet diverse needs of actual explorations. The signal from the main control board controls the output of the IPM after passing through the multi-channel optocoupler isolation device in order to reduce mutual interference between the signals. The DC–DC module converts the 5 V voltage into 15 V to provide the required DC voltage for regular operation of the IPM. The current is injected into the ground through the transmitting electrode of the transmitter board to observe the IP phenomenon of the ground medium; the voltage and current signals can be recorded simultaneously by the data acquisition board for post-acquisition data processing.

The versatility of the transmitter is crucial as different exploration environments and methods present different requirements for the transmitter [27], [28]. The transmitter developed in this study has a maximum output voltage of 1200 V and a maximum output current of 10 A, which can meet the power requirements of various environments (low power in the laboratory or high power in the field). In addition, it is equipped with over-voltage, over-current, and over-temperature protection circuits to ensure safety of the operators. The transmitter board can be used in conjunction with the data acquisition board (Section IV A) developed in this study, in addition to being used with other types of acquisition stations for various explorations. Fig. 9 shows the waveforms recorded at a transmitting frequency of 1 Hz, voltage of 900 V, and current of 4.5 A in an actual exploration; the accuracy of the transmitting current is approximately 1%.

D. MASTER CONTROL SOFTWARE

Python is a powerful, flexible, and extensible high-level computer language. It contains a complete set of corresponding standard library files, rendering programming more accessible. Developers can use C or C++ to add new modules or classes to Python. Accordingly, Python can also be embedded in C or C++ projects. In addition, the excellent cross-platform framework of Python renders it more compatible with conventional systems such as Windows and Linux [29], [30]. In this study, we used Python to develop the master control program of the IP instrument, which comprises several modules, including human–computer interaction, system monitoring, wireless communication, data storage and processing, transmission system control, and receiving system control. The human–computer interaction module responds by analyzing the different keying actions of the user and simultaneously uses various flashing frequencies and colors of LED lights to indicate the current working status of the system. The system monitoring module is responsible for real-time monitoring and reporting of the temperature, voltage, current, power, battery level, storage space, and working status of the system. The wireless communication module establishes Wi-Fi communication, data transmission, and command interaction between the instrument and the Android mobile device. The data storage and processing module is responsible for local SD card storage, real-time data calculation, and parameter display of the collected data. The transmission system control module enables users to adjust the transmission power and set parameters such as the transmission waveform and transmission time. The receiving system control module performs the following functions: channel self-test (uses signals inside the instrument to test whether the channel is operating normally before fieldwork commences), spontaneous potential compensation (reduces the potential difference between the receiving electrodes M and N), and automatic gain setting (adjusts the gain of the amplifier according to the amplitude of the acquisition signal).

The program adopts a top–down modular design scheme; the operation flow chart of the master program is shown in Fig. 10, which mainly includes network connection, project creation, parameter setting, and data processing and transmission. A project is first created when exploring a location in the field; then, the key parameters of the transmission and receiving systems are set. The real-time processed results, raw data, and parameters are saved in the project after measurement has been completed to facilitate post-acquisition data analysis.

E. REMOTE WIRELESS COMMUNICATION TECHNOLOGY

In recent years, the current state of relying on heavy cables for geophysical exploration has been alleviated owing to continuous advancement in communication technology. Communication technologies, including short-distance Bluetooth and IoT technologies, such as low-power IoT,

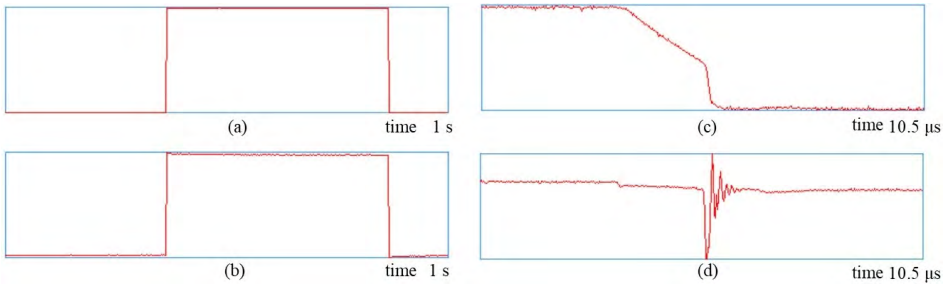

FIGURE 9. Waveforms recorded in an actual exploration: (a) voltage waveform, (b) current waveform, (c) voltage transition edge, and (d) current transition edge.

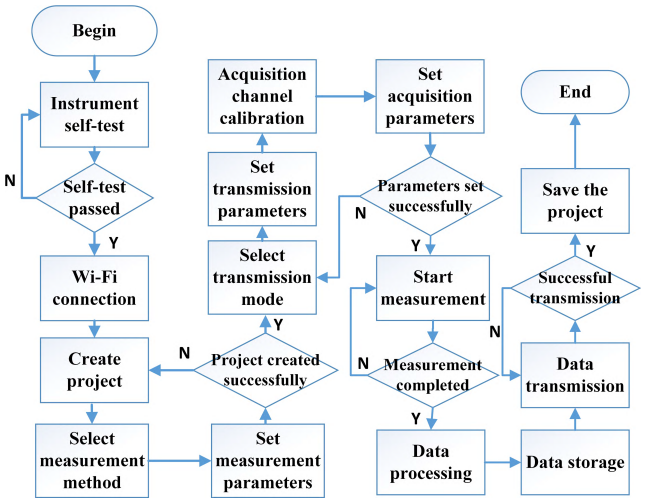

FIGURE 10. Operation flowchart of the master program of the IP instrument.

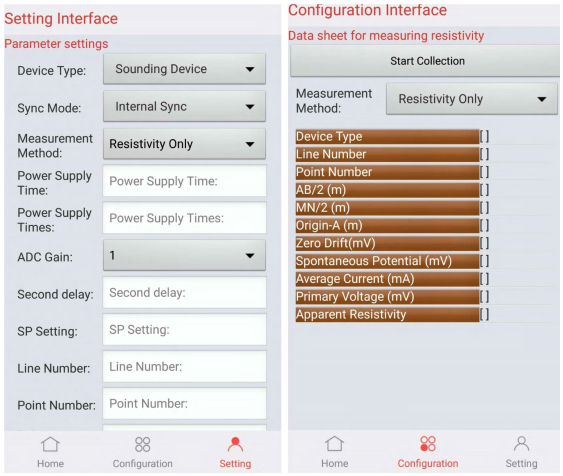

FIGURE 11. Partial interface of the host computer (left: Project setting interface, right: Data display interface during a single resistivity measurement).

Zigbee technology, and low- and medium-speed Wi-Fi transmission technologies, have been increasingly applied in geophysical instruments to improve the efficiency of field exploration and reduce the use of labor and resources [31]–[34]. In the proposed system, users can use Android mobile phones to perform remote wireless control of IP instruments through Wi-Fi. Communication between the mobile phone and the instrument is based on the TCP protocol, and the system achieved stable and reliable data transmission. The instrument receives and analyzes data from the Android host computer through the Wi-Fi module, and then performs appropriate actions and feeds the corresponding data back to the host computer terminal. The host computer is programmed in Java, and the software uses the Model-View-Presenter (MVP) design mode to separate the operation of the pages from the functional logic; the underlying Wi-Fi control module and the message delivery module of the software have high reusability, which allows convenient software upgrade and expansion. A partial interface of the host computer software is shown in Fig. 11.

Data quality monitoring is considerably important to improve the quality of data collected in the field and the reliability of exploration results. We provided two innovative remote data quality monitoring solutions. Fig. 12(a) shows the schematic diagram of remote monitoring based on the unique SMS functionality of BDS. It can transmit up to 120 Chinese characters at a time, and has advantages of bidirectional communication and low latency. After encrypting the message, the sender relays and transmits it to the ground central service station via a communication satellite. After receiving the satellite communication command, the central service station decrypts and re-encrypts the message, and then transmits it to the receiver by broadcasting via the communication satellite. Once the receiver decrypts the message, the receiving and transmitting processes of a message are complete [35], [36]. In addition, the communication circuit of the IP instrument, network port to 4G/5G module, and cloud service platform can be utilized to realize remote monitoring [37]. Each instrument can transmit relevant data to the cloud server over 4G/5G network (Fig. 12(b)). Users can use mobile phones, computers, and other terminals to monitor the operating status of each instrument remotely and control the instruments. When there is no carrier network in some remote environments, a local area network (LAN) can be constructed to realize long-distance and large-scale monitoring.

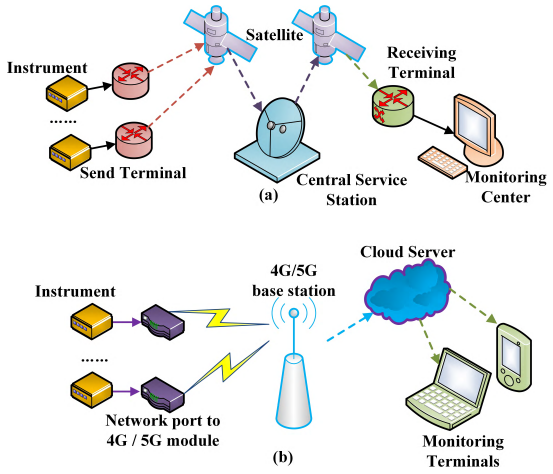

FIGURE 12. Schematic of the remote monitoring scheme of the IP instrument: (a) BDS SMS-based and (b) cloud service platform-based.

TABLE 1. Main performance indexes: summary and comparison.

INDEX	DEVELOPED IP INSTRUMENT	IPR-12 OF SCINTREX
Applicable method	TDIP, FDIP, Resistivity	TDIP, Resistivity
Function	Transmitter, Receiver	Receiver
Dimension	270×180×130 mm^3	355×270×165 mm^3
Weight	2 kg	7.1 kg
Noise floor	0.29 μV	50 μV
Maximum input voltage	10 V	14 V
Synchronous mode	Self-synchronization & GPS	Self-synchronization
Input impedance	30 MΩ	16 MΩ
Memory size	32 GB	400 dipoles
Data transmission method	Wireless (Wi-Fi or 4G/5G)	Wired (Serial port)
Maximum data transmission speed	>16 Mbps	57.6 Kbps
Human–computer interaction mode	Advanced Android device	Traditional buttons and LCD screen
Battery type	Lithium battery	Nickel-cadmium battery

F. PERFORMANCE SUMMARY AND COMPARISON

A comparison of the main performance indexes of the IP instrument system developed in this study and that of IPR-12 of Scintrex is presented in Table 1.

V. INSTRUMENT TESTS

A. LABORATORY TESTS

We first investigated whether the transmitter and receiver are operating normally. During the test, a 20 Ω resistor was used as the transmitter load, and the receiver collects signals at both ends of the resistor. Fig. 13 shows the waveform drawn using MATLAB based on data collected when the power

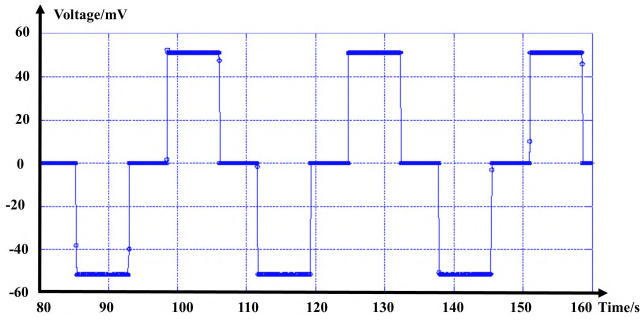

FIGURE 13. Transmitter waveform for a pure resistive load.

supply voltage is 60 mV and the power supply level time is 4 s. The figure shows that when a pure resistive load is used, the operations of the transmitter and receiver are stable, and the output waveform is ideal without obvious glitches. This demonstrates that the receiver can accurately collect the signal, and that the IPM module circuit can effectively suppress noise and overcome the impact of impulse current on the acquisition circuit at the moment of switch opening and closing. Then, we changed the load resistance to polarizable bodies and conducted several flume experiments. Copper plates were used as the transmitting electrodes A and B, and the measured specimens (steel plates or copper plates) were placed 2–3 cm below the water surface in the middle of the flume. Platinum nonpolarized electrodes were used as the receiving electrodes M and N to collect signals from both ends of the specimen. Fig. 14 shows the time spectrum curves when steel plates are used as the measured polarizable body. The figure shows that immediately after turning on the power supply, the voltage difference rapidly increases to form a primary field. With the increase in the power supply time, the voltage difference gradually increases and finally reaches a stable value of 15 mV. After the power supply has been turned off, the potential difference of the secondary field rapidly drops to 5 mV at the instant of power failure, and then the rate of decrease gradually slows, and the final attenuation is zero. This indicates stable operation of the instrument and that it accurately reflects the charging and discharging characteristics of the polarization phenomenon.

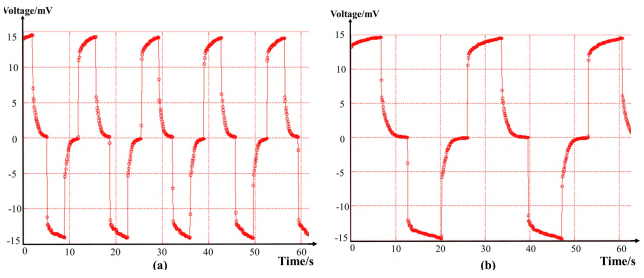

FIGURE 14. IP curves of steel plates in the flume experiment: (a) 4 s level time of power supply and (b) 8 s level time of power supply.

B. CAMPUS EXPERIMENT

To test whether the instruments are operating normally and that they are collecting signals accurately in environments

with severe interference, we conducted many outdoor experiments in a school campus that has various interference sources that are worse than in a wild environment. During the experiments, the transmitting voltage was fixed, the distance between the receiving electrodes M and N was varied, and the voltage change of the secondary field was recorded. In one of the experiments, the ratio of the distance between the receiving electrodes M and N and the transmitting electrodes A and B was 1:5. The collected secondary field data were analyzed and processed in MATLAB; Fig. 15 shows the attenuation curves of the secondary field. The figure shows that all the voltage values of the secondary field decrease rapidly from a large value (a: 40 mV b: 20 mV), and then gradually approach a smaller stable value (a: ∼0 mV b: 5 mV). In Fig. 15(b), the distances between A and B and M and N are relatively large (AB: 30 m MN: 6 m). The recorded stable value (5 mV) of the secondary field is smaller than that in Fig. 15(a) (∼0 mV) owing to some strong interference, which is expected in a field environment. We can further improve the quality of data acquisition by improving the transmission power or reducing the distance.

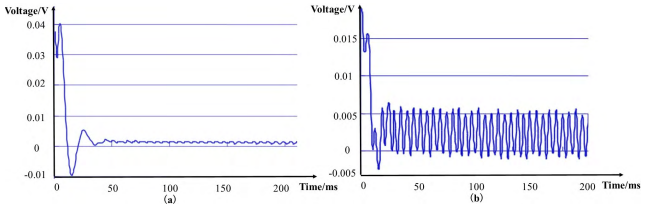

FIGURE 15. Attenuation curves of the secondary field in campus experiments: (a) 1 m between M and N and (b) 6 m between M and N.

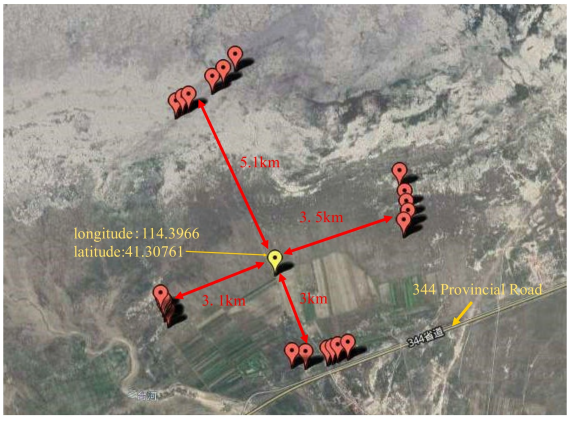

FIGURE 16. Location distribution of each instrument.

C. WIRELESS COMMUNICATION TESTS

To verify the feasibility of the remote wireless communication solutions, we conducted a long-distance networking experiment with multiple instruments in the field. The location distribution of each instrument is shown in Fig. 16. The red markings in the figure represent the instruments and

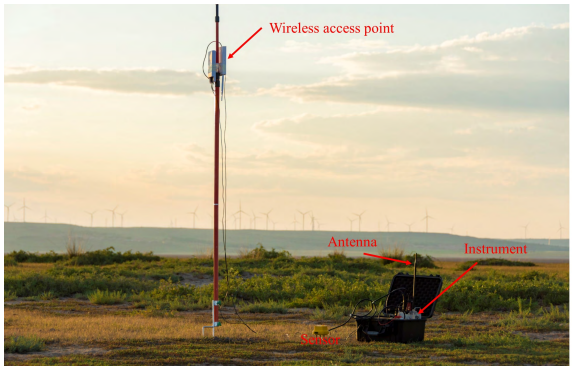

FIGURE 17. Photograph showing the instrument in field experiment.

the yellow marking represents the location of the monitoring center. Several instruments are located around the monitoring center at a distance of more than 3 km; the farthest distance was more than 5 km. We built a LAN using the Wi-Fi communication function of the instrument and the related communication equipment as there is no carrier network in this area. Fig. 17 shows a photograph of the field work. The bathymetric and joint profile results of one of the lateral lines obtained by real-time processing of data transmitted wirelessly from the instruments are shown in Fig. 18. It can be observed from the bathymetric map that the resistivity can be clearly divided into two regions, namely low resistivity and high resistivity, at 280 m. A high resistance concentration trap can be observed from the high resistance region, with a center of (330 m, –30 m). The intersection of ρA and ρB is found at almost the same location through analysis of the results of the joint section, and it is concluded that this location is likely to be the central location of the anomalous body. In the joint profile, $\rho A > \rho B$ when the measuring line is greater than 330 m and $\rho A < \rho B$ when it is less than 330 m, but the peak resistivity difference between the two sides is large. Therefore, it is concluded that there may be an inclined geological body or lithologic boundary. Experimental results show that our LAN wireless communication solution can realize real-time data transmission within a range of 5 km at a speed of approximately 8 Mbps, which fully meets the requirements of high-speed data transmission and long-distance real-time monitoring.

D. COMPARATIVE FIELD EXPERIMENTS

To verify the consistency and reliability of the actual field results of the developed instruments, we conducted several additional field experiments. Fig. 19 and Fig. 20 show the apparent resistivity and apparent polarizability maps obtained from field experiments conducted using our two IP instruments and the commercial instrument DZD-6A at the same location in a suburb of Hebei Province. It can be observed from the figure that the results of the three instruments are highly consistent. In fact, the error of the data measured using our instruments is no more than

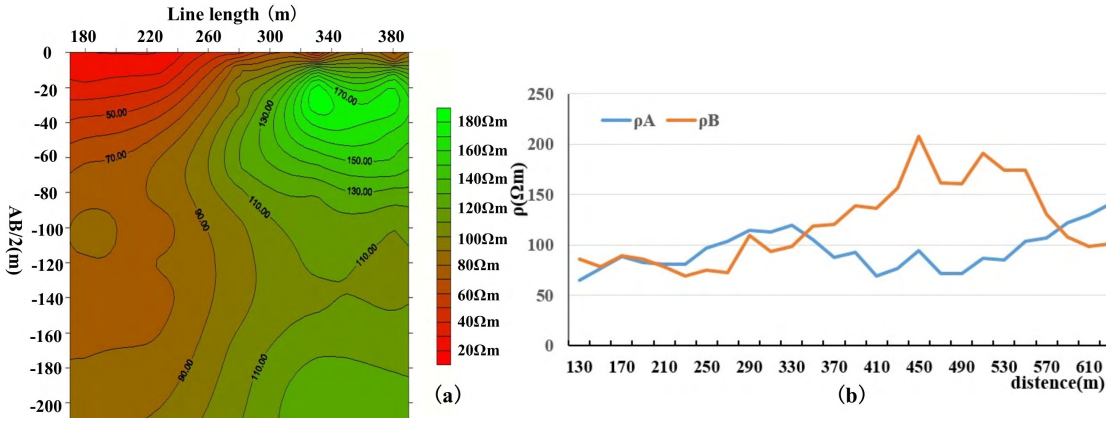

FIGURE 18. Results obtained by processing data in real time: (a) bathymetric result and (b) joint profile result.

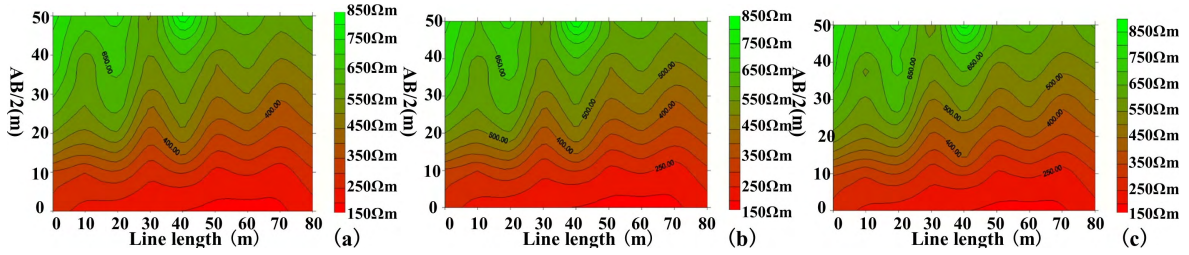

FIGURE 19. Comparison of apparent resistivity results: (a) IP instrument No. 1, (b) IP instrument No. 2, and (c) DZD-6A.

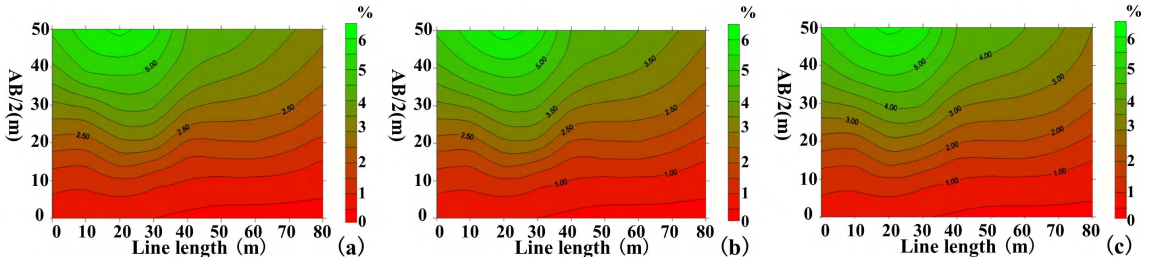

FIGURE 20. Comparison of apparent polarizability results: (a) IP instrument No. 1, (b) IP instrument No. 2, and (c) DZD-6A.

0.5% compared with that of DZD-6A, indicating that our instrument has good consistency and high reliability of exploration results. Further analysis of the results showed that the apparent resistivity is low ($< 300\ \Omega \cdot m$) in the near surface area. Furthermore, it generally exhibits an increasing trend with the increase in the detection depth. When the detection depth reaches 40–50 m, the apparent resistivity of the region near the position of 0 m is large; however, a small lateral fluctuation occurs, and abnormal geological bodies may be present. The near surface apparent polarizability is low (<2%), and the maximum value (∼5.5%) occurs at (20 m, 50 m) where abnormal geological bodies may be present. We preliminarily considered that the area centered at (20 m, 50 m) may consist of small amounts of metallic ore because metallic minerals usually exhibit low resistivity and high polarizability.

VI. CONCLUSION

A novel multifunctional IP instrument system based on remote wireless communication technology with advantages of high integration, high data acquisition accuracy, multi-function capability, compact, lightweight, convenient operation, and a high degree of intelligence was developed in this study. We explored the following key technologies in the system to address the problems found in most existing IP instruments, namely limited acquisition accuracy, large size, separate transmitter and receiver, complex human–computer interaction, difficult networking, and remote monitoring.

(1) Circuit design of a high-precision data acquisition board. The circuits of pre-amplification, low-pass filtering, single-ended to differential, and analog-to-digital conversion were designed based on the characteristics of the collected

signals. The test results showed that the noise floor of the data acquisition circuit was 0.29 μV.

(2) Design of a filter to reduce the 50 Hz utility frequency interference. Low-cost operational amplifiers and resistor–capacitors were used to construct a 50 Hz filter circuit with a notch filter depth exceeding 40 dB. The circuit can be used in conjunction with a digital software filter; the 50 Hz interference can be reduced to 80 dB.

(3) Design of the multifunctional high-power transmitter. A multifunctional transmitter board was designed and constructed using an IPM core; the maximum output power was 6 kW, and it can transmit step waves (time domain) or rectangular waves (frequency domain) with various frequencies and duty cycles. It was equipped with over-temperature, over-current, and over-voltage protection circuits to ensure safety of users.

(4) Master control software design based on Python. Python was used in this study to develop the master control program of the IP instrument. A top–down modular design was adopted, comprising several modules, including human–computer interaction, system monitoring, wireless communication, data storage and processing, and transmission and receiving system control.

(5) Design of the remote wireless communication scheme. We introduced the IoT technology in the IP instrument. Users can use Android mobile phones to control the instrument through a Wi-Fi network, and can use the unique SMS functionality of BDS or the cloud service platform to establish remote data quality monitoring of multiple instruments in a wide area.

The results of multiple experiments demonstrate that the functions and indexes of the instrument satisfy the expected requirements. However, it is not currently possible to acquire multiple channels of data simultaneously because the acquisition board is a single-channel. In the future, we will continue to improve and upgrade the instrument, such as modifying the single-channel data acquisition board into a multi-channel board to improve the exploration efficiency and the functions of the transmitter to increase the transmission power and enhance its anti-interference capability. Moreover, medical instruments can employ the low-noise data acquisition circuit developed in this study to improve the accuracy of weak bioelectrical signal acquisition and medical imaging. The wireless communication technology proposed in this study provides a reference for joint work and networking of multiple medical instruments, thereby enhancing the efficiency of real-time imaging and intelligence of the instruments [38].

ACKNOWLEDGMENT

The authors would like to thank S. Song, B. Qiao, and D. Zhang for data processing and field tests. They would also like to thank Editage for English language editing.

REFERENCES

[1] J. M. Li, *Geoelectric Field and Electrical Exploration*. Beijing, China: GEO Public House, 2005.
[2] L. Cagniard, "Basic theory of the magneto-telluric method of geophysical prospecting," *Geophysics*, vol. 18, no. 3, pp. 605–635, 1953.
[3] C. Wang and L. D. Slater, "Extending accurate spectral induced polarization measurements into the kHz range: Modelling and removal of errors from interactions between the parasitic capacitive coupling and the sample holder," *Geophys. J. Int.*, vol. 218, no. 2, pp. 895–912, Aug. 2019.
[4] H. Vanhala, "Mapping oil-contaminated sand and till with the spectral induced polarization (SIP) method," *Geophys. Prospect.*, vol. 45, no. 2, pp. 303–326, Mar. 1997.
[5] F. Zarif, P. Kessouri, and L. Slater, "Recommendations for field-scale induced polarization (IP) data acquisition and interpretation," *J. Environ. Eng. Geophys.*, vol. 22, no. 4, pp. 395–410, 2017.
[6] J. S. He, "Measurement precision of induced polarization method and its effect on application," *Geophys. Geoche. Explor.*, vol. 19, no. 1, pp. 41–47, 1995.
[7] H. Jang, H. J. Kim, and M. J. Nam, "In-loop transient electromagnetic responses with induced polarization effects of deep-sea hydrothermal deposits," *IEEE Trans. Geosci. Remote Sens.*, vol. 54, no. 12, pp. 7272–7278, Dec. 2016.
[8] G. Fiandaca, E. Auken, A. V. Christiansen, and A. Gazoty, "Time-domain-induced polarization: Full-decay forward modeling and 1D laterally constrained inversion of cole-cole parameters," *Geophysics*, vol. 77, no. 3, pp. E213–E225, May 2012.
[9] B. Q. Qiao, "The study and design on time domain spectral induced polarization instrument," Ph.D. dissertation, School Geophys. Inf. Technol., China Univ. Geosci., Beijing, China, 2009.
[10] G. D. Liu, "Promote the innovation of geophysical methodology, and lead the future of exploration apparatus technology," *Chin. J. Geophys.*, vol. 60, no. 11, pp. 4145–4148, 2017.
[11] Phoenix Geophysics. *V8 RECEIVER*. Accessed: Feb. 1, 2020. [Online]. Available: http://www.phoenix-geophysics.com/products/receivers/v8
[12] IRIS. (2020). *I-FullWaver*. Accessed: Feb. 1, 2020. [Online]. Available: http://www.iris-instruments.com/i-fullwaver.html
[13] Q. Y. Di, G. Y. Fang, and Y. M. Zhang, "Research of the surface electromagnetic prospecting (SEP) system," *Chin. J. Geophys.*, vol. 56, no. 11, pp. 3629–3639, 2013.
[14] Q. Y. Jiang, "Study on the key technology of wide field electromagnetic sounding instrument," Ph.D. dissertation, School Earth Sci. Inf. Phys., Central South Univ., Changsha, China, 2010.
[15] R. J. Chen, "The study on pseudo-random multi-frequency electromagnetic prospecting system," Ph.D. dissertation, School Inf. Phys. Eng., Central South Univ., Changsha, China, 2003.
[16] S. He, *Wide-Area Electromagnetic Method and Pseudo-Random Signal Method*. Beijing, China: Higher Education Press, 2010.
[17] G. HI-Technology. *SQ-5 Dual-Frequency IP Instrument*. Accessed: Apr. 10, 2020. [Online]. Available: http://www.geosun.com.cn
[18] LAUREL. *IPR-12*. Accessed: Apr. 10, 2020. [Online]. Available: https://www.laureltechnologies.com/wp-content/uploads/2016/11/IPR-12.pdf
[19] ORANGELAMP. *GDD*. Accessed: Apr. 10, 2020. [Online]. Available: https://www.orangelamp.com.cn/instrument/product/c_18-1.html
[20] Q. S. Zhang, M. Deng, Q. Wang, Y. Q. Feng, and R. Yang, "Application of embedded technology for induced polarization instrument," *Adv. Mater. Res.*, vols. 383–390, pp. 224–229, Nov. 2011.
[21] G. F. Deng, "Research and implementation of dual frequency induced polarization receiver based on FPGA," Ph.D. dissertation, Guilin Univ. Electron. Technol., Guilin, China, 2018.
[22] A. Williams, *Analog Filter and Circuit Design Handbook*. Beijing, China: House of Electronics Industry, 2016.
[23] S. C. Ge, M. Deng, K. Chen, B. Li, and Y. Li, "Improved data preprocessing algorithm for time-domain induced polarization method with digital notch filter," *Acta Geophysica*, vol. 64, no. 6, pp. 2263–2287, Dec. 2016.
[24] A. Agarwal, J. H. Lang, *Basics of Analog and Digital Electronic Circuits*. Beijing, China: Tsinghua Univ. Press,2008.
[25] Y. B. Wang and J. S. He, "Development and application of the WSJ-4 multifunction digital IP instrument receiving system based on pseudo-random signal," *Geophys. Geochemical Explor.*, vol. 38, no. 5, pp. 1012–1017, 2014.
[26] M. Li, *Technical Guide to Induced Polarization Methods*. Beijing, China: GEO Public House, 2004.
[27] M. Wang, S. Jin, M. Deng, W. Wei, and K. Chen, "Multifunction electromagnetic transmitting system for mineral exploration," *IEEE Trans. Power Electron.*, vol. 33, no. 10, pp. 8288–8297, Oct. 2018.

[28] X. Zeng, M. Wang, S. Jin, H. Duan, and K. Chen, "Arbitrary frequency table transmission technology for a high-power borehole–ground electromagnetic transmitter," *IEEE Access*, vol. 6, pp. 11502–11507, 2018.
[29] A. F. J. López, M. C. P. Pelayo, and Á. R. Forero, "Teaching image processing in engineering using Python," *IEEE Revista Iberoamericana de Tecnologias del Aprendizaje*, vol. 11, no. 3, pp. 129–136, Aug. 2016.
[30] Q. G. Ruan, "Visual aids drive system design and implementation based on Python language and ARM," Ph.D. dissertation, School Inf. Sci. Eng., Central South Univ., Changsha, China, 2014.
[31] L. Shu, M. Mukherjee, L. Hu, N. Bergmann, and C. Zhu, "Geographic routing in duty-cycled industrial wireless sensor networks with radio irregularity," *IEEE Access*, vol. 4, pp. 9043–9052, 2016.
[32] W. H. Li, Q. S. Zhang, Q. M. Zhang, F. Guo, S. Q. Qiao, S. Y. Liu, Y. Y. Luo, Y. F. Niu, and X. Heng, "Development of a distributed hybrid seismic–electrical data acquisition system based on the Narrowband Internet of Things (NB-IoT) technology," *Geosci. Instrum. Methods Data Syst.*, vol. 8, no. 2, pp. 177–186, Aug. 2019.
[33] S. Qiao, H. Duan, Q. Zhang, Q. Zhang, S. Li, S. Liu, S. Liu, Y. Wang, S. Yan, W. Li, and F. Guo, "Development of high-precision distributed wireless microseismic acquisition stations," *Geosci. Instrum., Methods Data Syst.*, vol. 7, no. 3, pp. 253–263, Sep. 2018.
[34] S. Qiao, Q. Zhang, and Q. Zhang, "Mine fracturing monitoring analysis based on high-precision distributed wireless microseismic acquisition station," *IEEE Access*, vol. 7, pp. 147215–147223, 2019.
[35] Q. P. Wang, J. Xiao, C. Zheng, Y. Z. Lin, Y. Zheng, and S. J. Zhang, "Design and implementation of multi-point tracking system based on Beidou short message," *J. Appl. Oceanogr.*, vol. 38, no. 1, pp. 135–140, 2019.
[36] H. S. Chen, X. Y. Guo, F. Wang, and H. S. Lu, "Fishery harvesting information compressing and transmitting method based on Beidou short message," *Trans. Chin. Soc. Agricult. Eng.*, vol. 31, no. 22, pp. 155–160, 2015.
[37] M. Peng, C.-L. I, C.-W. Tan, and C. Huang, "IEEE *ACCESS* special section editorial: Recent advances in cloud radio access networks," *IEEE Access*, vol. 2, pp. 1683–1685, 2014.
[38] M. Nasiriavanaki, J. Xia, H. Wan, A. Q. Bauer, J. P. Culver, and L. V. Wang, "High-resolution photoacoustic tomography of resting-state functional connectivity in the mouse brain," *Proc. Nat. Acad. Sci. USA*, vol. 111, no. 1, pp. 21–26, Jan. 2014.

WENHAO LI was born in Henan, China, in 1996. He received the B.E. degree in measurement and control technology and instrumentation from the China University of Geosciences (Beijing), Beijing, in 2018, where he is currently pursuing the master's degree. His main research interests are geophysical instrumentals, and control science and engineering.

QISHENG ZHANG was born in Anhui, China, in 1978. He received the Ph.D. degree from the China University of Geosciences (Beijing), Beijing, in 2012. He is currently an Associate Professor with the School of Geophysics and Information Technology, China University of Geosciences (Beijing). His research interests include system-on-a-programmable-chip technology, measurement technology and instrumentation, high precision data converters, and geophysical instruments.

YUEYUN LUO was born in Hunan, China, in 1996. He received the B.E. degree in measurement and control technology and instrumentation from the China University of Geosciences (Beijing), Beijing, in 2018, where he is currently pursuing with master's degree. His main research interest is geophysical instrumentals.

QIMAO ZHANG was born in Anhui, China, in 1987. He received the M.S. degree from the China University of Geosciences (Beijing), Beijing, in 2012. He is currently an Assistant Researcher with the Institute of Electronics, Chinese Academy of Sciences (IECAS). His main research interest is electromagnetic instruments.

FEI JIANG was born in Anhui, China, in 1997. She received the B.E. degree in exploring technology and engineering from the China University of Geosciences (Beijing), Beijing, in 2019. She is currently pursuing the master's degree with the University of Science and Technology of China. Her main research interest is geodynamics.